Chemistry - Methods

Chemistry—Methods

Chemistry Europe
European Chemical Societies Publishing

RESEARCH ARTICLE OPEN ACCESS

Lanthanide Monoporphyrinates and Complexes With a Schiff Base Derivative: Thermodynamic Stability and Bioimaging Capabilities

Wanqi Zhou[1,2] | Boyang Li[2] | Qian Zhang[1] | Chen Xie[1] | Jean-Claude G. Bünzli[1,3] | Ka-Leung Wong[1,4]

[1]Department of Applied Biology and Chemical Technology, The Hong Kong Polytechnic University, Hong Kong SAR, China | [2]Department of Chemistry, Hong Kong Baptist University, Hong Kong SAR, China | [3]Institute of Chemical Sciences and Engineering, Swiss Federal Institute of Technology, Lausanne, Switzerland | [4]Department of Chemistry, City University of Hong Kong, Hong Kong SAR, China

Correspondence: Chen Xie (chen-polyu.xie@polyu.edu.hk) | Jean-Claude G. Bünzli (jean-claude.bunzli@epfl.ch) | Ka-Leung Wong (klwong@cityu.edu.hk; klgwong@polyu.edu.hk)

Received: 27 February 2026 | **Revised:** 1 April 2026 | **Accepted:** 3 April 2026

Keywords: Bioimaging; NIR | Lanthanides | Luminescence | Porphyrinate | Schiff base | Stability constants

ABSTRACT

Clinical applications ranging from magnetic resonance imaging to cancer therapy are more relying on the use of lanthanide coordination compounds. However, the coordination properties based on the electronic configuration of lanthanide ions can be easily sequestered by serum proteins and consequently induce unwanted side effects and/or toxicity if leaked from the bioprobe/prodrug. The knowledge of the thermodynamic and kinetic stability of the complexes used in these applications is therefore essential. To close this gap, we present here the determination of the stability constants via spectrometric method of three lanthanide monoporphyrinates capped with Kläui's ligand, **LnL1** (Ln = Gd, Er, Yb), whose stability has not been studied yet, under physiological conditions (37 °C, pH 7.5); the monoporphyrinates are found to be more stable than corresponding EDTA chelates, but significantly less stable than corresponding macrocyclic DOTA chelates. In addition, we turn our attention to less stable bimetallic chelates with a Zn-containing Schiff base derivative, **LnL3** (Ln= Nd, Gd, Yb, LogK_C = 4.8–5.1), and explore the potentiality of **LnL1** and **LnL3** complexes as NIR imaging probes.

1 | Introduction

Lanthanide coordination compounds are widely used in modern clinical applications, with established roles in cancer diagnostic imaging and therapy, including photodynamic therapy and radiotherapy [1]. Moreover, the distinct photophysical properties of lanthanide ions, including narrow emission bands, long lifetimes, and minimal background interference, have driven considerable research into their utility as optical bioimaging probes. However, due to the Laporte forbidden electric dipole 4f-4f transitions, lanthanide ions typically exhibit very weak absorption, making them difficult to excite. A common strategy to overcome this drawback is the use of small-molecule photosensitizers, which excite lanthanide ions through energy transfer (antenna effect) [2]. These photosensitizers are either directly chelated to the metal ion or grafted onto the chelating ligand [3]. Lanthanide luminescent probes are ubiquitous in medical analysis, for instance, in time-resolved luminescence immunoassays, often based on luminescence resonant energy transfer, which allow not only the quantitation of antibodies and proteins but also the study of their dynamics [4].

Regarding clinical applications, well-known examples are the class of gadolinium-based contrast agents (GBCAs) used in magnetic resonance imaging (MRI), where the toxic Gd^{3+} ion is safely administered by being strongly chelated with linear or macrocyclic polyaminocarboxylate ligands [5]. In addition, lanthanum carbonate has been used since its 2004 approval by the FDA

for reducing phosphate levels in end-stage renal disease patients, and another FDA-approved drug is Pluvicto (^{177}Lu vipivotide tetraxetan) for radionuclide therapy toward prostate-specific membrane antigen-positive metastatic castration-resistant prostate cancers [6, 7].

Despite their utility, lanthanides carry certain risks in clinical use. In rare, specific cases, lanthanide ions have been linked to severe side effects after frequent use [8]: a notable case which emerged in the early 21st century is the association between GBCAs and nephrogenic systemic fibrosis (NSF) in patients with kidney dysfunction [9], which brought lanthanide safety into public focus. The toxicity of free lanthanide ions can be primarily attributed to two factors: (1) the coordination chemistry similarity to calcium ions, which can lead to their sequestration by serum proteins, and (2) the formation of insoluble precipitates when they interact with anions commonly found in biological media like carbonate or phosphate [10, 11]. These two factors significantly extend the retention of lanthanides within the body after drug uptake. Consequently, the knowledge of the thermodynamic stability of lanthanide complexes used as drugs is critical for assessing the amount of metal ion leakage and is a fundamental parameter in evaluating overall toxicity.

Current approaches to reach the stability constants include potentiometry and spectrometry. Potentiometry measures the stability constant according to the change of the solution potential during the titration, which can provide the information for calculating the binding site in the process [12, 13]. Spectrometry focuses on the quantification of components that contain a chromophore. Spectrometric measurement is more species-specific.

Common ligands for designing lanthanide bioprobes and/or prodrugs include Schiff bases [14] and porphyrinates [15]. Porphyrins are common photosensitizers consisting of a tetrapyrrolic macrocycle with a large conjugation system, facilitating the generation of reactive oxygen species [16]. While complexes with tetrapyrroles are widely used in many applications in view of their presumed large stability, complemented by specific magnetic and photophysical properties [16], to the best of our knowledge, no stability constants have been reported to date for this class of chelates. To fill up this gap and to compare with polyaminocarboxylates, we present the first study on the stability of lanthanide monoporphyrinates (**LnL1**) as shown in Figure 1. In this work, we chose a well-studied tetrapyrrolic system grafted with 4-methylpyridinium groups onto the *meso*- positions to enhance water solubility in this study, with resulting positive charges compensated by iodide anions. Porphyrins act as a tetradentate ligands and do not saturate the coordination sphere of lanthanide ions, which often have large coordination numbers [17]. Therefore, to obtain stable monoporphyrinate complexes, Kläui's ligand [18] was used as a capping unit to complete the coordination sphere of the lanthanide ions. The modifiable phosphite substituents of the Kläui ligand provide the alternation of solubility [15].

We also turn our attention to less stable Schiff base complexes (**LnL3**) to investigate if the photophysical properties of lanthanide complexes can be correlated with their bioimaging ability. The salen-type ligand chosen belongs to a family of Schiff-base ligands obtained by reacting o-vanillin with a diamine. The resulting bicompartmental, hexadentate molecule is ideally suited for building 3d-4f heterometallic complexes that have adequate antenna effects for visible- and NIR-emitting lanthanide ions [19–21] Stability constants were obtained via direct or competitive spectrophotometric titration methods with the octadentate corresponding macrocyclic (**LnL2**) and linear polyaminocarboxylates (**LnL4**), whose stability with lanthanides [22, 23] is quantitatively well known, which makes them ideal competitors for stability constant determination. The studied ions include Gd^{+3} in view of its role in MRI contrast agents and the NIR-emitting Nd^{3+}, Er^{3+}, and Yb^{3+} ions, since present trends focus on optical bioprobes emitting in

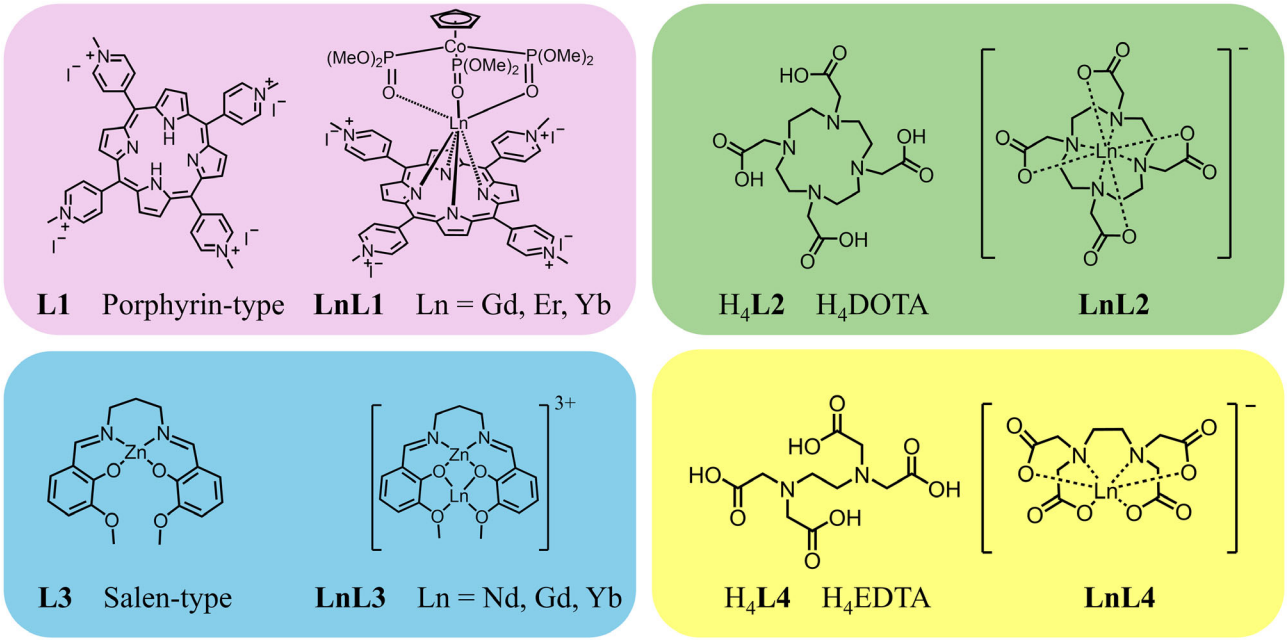

FIGURE 1 | Chemical structures of the lanthanide complexes LnL1 and LnL3 studied in this work and of reference anionic complexes LnL2- (LnL2) and LnL4- (LnL4). Chelating structures: L1 (Porphyrin-type): 5,10,15,20-tetrakis(N-methyl-pyridinium-4yl)−21,23H-porphyrin tetraiodide; L2, DOTA: 2,2′, 2″, 2‴- (1,4,7,10-tetraazacyclododecane-1,4,7,10-tetrayl)tetraacetic acid); L3 (Salen-type): [N, N'-bis(3-methoxysalicylidene)propane-1,3-diamine] zinc(II); L4, H4EDTA: ethylenediamine tetraacetic acid (2,2′, 2″, 2‴-(ethane-1,2-diyldinitrilo)tetraacetic acid).

the NIR-I and NIR-II biological windows [24]. The luminescent properties of the lanthanide complexes were analyzed under different conditions, including a cell-cultured environment and the presence of interfering ions, to unravel the potential relationship between complex stability and bioimaging capability.

2 | Results and Discussion

2.1 | Stability Constants

Figure 2 shows the photophysical properties of the NIR-emissive complexes **YbL1** and **NdL3**, and of their corresponding ligands. The spectra of the porphyrin compounds show a significant red shift between the absorption of the ligand and of the ytterbium complex, which can be used to determine the speciation in solution. The most intense absorption bands at 422 and 441 nm of **L1** and **YbL1**, respectively, refer to the 'Soret' band (Figure 2a) [25]. The much weaker Q bands appear in the 500–700 nm range. When excited at 420 nm, the free porphyrin **L1** generates a broad emission from 600 to 800 nm peaking at 670 nm (Figure 2b) that almost completely vanishes for the Yb^{3+} complex, due to energy transfer, with emission in the NIR around 1000 nm ($^2F_{5/2} \rightarrow {}^2F_{7/2}$ transition) (Figure 2c).

The absorption spectrum of the salen-type ligand (**L3**) (Figure 2d) is weak, due to small solubility; it displays three bands at 261, 297, and 419 nm assigned to $\pi \rightarrow \pi^*$ transitions. Upon coordination with Nd^{3+}, two main bands remain, at 266 nm, with shoulders at 279 and 341 nm. Upon excitation at 355 nm, a broad emission band is observed, with a maximum at 462 nm for **L3** (Figure 2e), while this band is absent for the complex, pointing to efficient energy transfer to the neodymium ion. The sharp and weak emission band at around 400 nm corresponds to the Raman band of the water stretching vibration (Figure 2e inset). In the NIR range (Figure 2f), emission bands at 900, 1062, and 1334 nm are observed that can be assigned to $^4F_{3/2} \rightarrow {}^4I_{9/2}$, $^4F_{3/2} \rightarrow {}^4I_{11/2}$, and $^4F_{3/2} \rightarrow {}^4I_{13/2}$ transitions of Nd^{3+} [21].

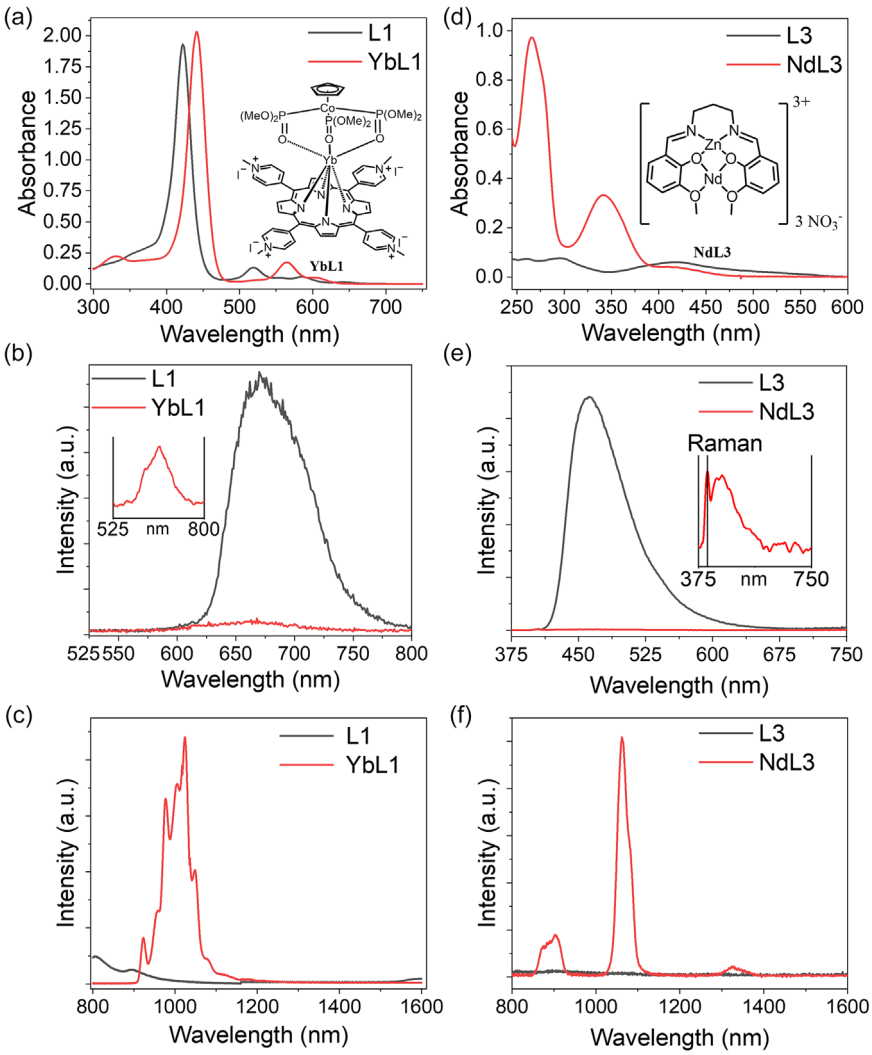

FIGURE 2 | Photophysical properties of lanthanide complexes and their corresponding ligands. (a) Absorption, (b) visible emission, and (c) NIR emission spectra of the porphyrin-based ligand **L1** (10 μM in 20 mM Tris, 150 mM NaCl, pH 7.5, $\lambda_{exc} = 420$ nm) and its ytterbium complex **YbL1** (10 μM in 20 mM Tris, 150 mM NaCl, pH 7.5, $\lambda_{exc} = 420$ nm). (d) Absorption, (e) visible emission, and (f) NIR emission spectra of the salen-based ligand **L3** (50 μM in 20 mM Tris, 150 mM NaCl, pH 7.5, $\lambda_{exc} = 355$ nm) and its neodymium complex **NdL3** (50 μM in 20 mM Tris, 150 mM NaCl, pH 7.5, $\lambda_{exc} = 355$ nm). Insets in (b) and (e) show magnified views of the visible emission for **YbL1** (165x magnification) and **NdL3** (256x magnification), respectively.

Since the NIR emission intensity may not be linearly proportional to concentration [26], we turned to the absorption spectra for the determination of the stability constants. Two different protocols were used, depending on the stability of the complexes (Figure S24a) direct measurement and the competing method. The direct method involves the spectrophotometric monitoring of absorption bands to quantify the concentrations of the metal complex. By applying the Beer–Lambert law to these measured absorbance values, we can directly calculate both the dissociation rate constants and the thermodynamic stability constants. However, a direct method cannot be applied to the measurement of the stability constant of the Ln-porphyrin-based complexes, as they are highly stable. Their kinetic inertness requires an impractically long duration to reach thermodynamic equilibrium. The spectrometer cannot detect the subtle absorbance changes occurring in a short period, as the changes could be masked by instrumental noise or baseline drift, making it impossible to accurately calculate the stability constant. Therefore, a competition strategy was selected with ethylenediaminetetraacetate disodium salt (Na_2-EDTA) as the competing ligand. The final equilibrium involving 5 components, Ln^{3+}, **LnL1**, **L1**, $EDTA^{2-}$, and Ln-EDTA (**LnL4**) was reached after a long time, over 90 days (Figure S24b), pointing to very slow ligand exchange kinetics, as expected for this type of macrocyclic complexes. Calculation of the stability (association) constant defined by Equation (2) was made using Equation (6) (see Experimental Section): linear regression of the log plot yields the difference between the stability constant of the complex with the competing ligand and the stability constant of **LnL1** (Figure S25–20). The data obtained are reported in Table 1. They point to the porphyrin complexes being 1–2 orders of magnitude more stable than EDTA chelates, but 4–7 orders of magnitude less stable than DOTA complexes. One of the reasons for better stability compared with EDTA is related to the cyclic structure of porphyrin, which has a pre-organized conformation for metal binding, while **L3** is a semi-preorganised open ring. Kläui's cap also helps to satisfy the coordination number of the trivalent lanthanide and enhances the stability of the monoporphyrinates. [15, 29, 30]

The stability constants of the salen-type complexes (**LnL3**) have been measured directly, as they are not very stable, while the stability constant can be calculated via dissociation without a third additive. The absorption spectra were measured immediately after dissolution in water and then were monitored for 10 days, the time needed to reach equilibrium. The absorption at both 265 and 345 nm decreases with time, and considering the negligible absorption of the ligand at 345 nm, this absorption can be used for quantifying the complex concentration. The extracted constant $\log K_C$ for **NdL1** is 4.82 ± 0.20. Using the same method, $\log K_C$ for the other two lanthanides was found slightly larger (Table 1), in line with increasing electron density on the metal ion as well as the lanthanide contraction [31]. Furthermore, the stability constants exhibit a progressive increase across the lanthanide series. We attributed this trend to the lanthanide contraction, where the decreasing ionic radii and increasing charge density of the heavier Ln^{3+} ions facilitate stronger electrostatic interactions and a superior fit within these pre-organized chelating cavities.

2.2 | Imaging Capability

To assess the influence of the stability of NIR-emitting lanthanide complexes on their imaging feasibility, emission spectra were measured in three different solvents, including water, phosphate buffer saline (PBS), and the cell culture minimum essential medium (MEM); they are displayed in Figure 3.

The **YbL1** macrocyclic complex remained NIR-emissive in all 3 solvents upon excitation at 420 nm. However, because the MEM background emission is also excited at this wavelength (Figure 3a), this causes a decrease in Yb^{3+} emission in this medium (Figure 3b) with absorption overlapping. On the other hand, the Nd^{3+} emission was almost quenched when **NdL3** was dissolved into PBS and MEM, while the ligand emission in the visible was enhanced significantly (Figure 3d-e). These changes suggest that Nd^{3+} dissociates from the light-harvesting ligand in a biological environment.

To test the feasibility of the lanthanide complexes for bioimaging, the luminescent spectra were further measured after the addition of large amounts of different potentially interfering cations, which are common trace elements in the human body.

In the case of **YbL1,** the addition of Mg^{2+}, Ca^{2+}, Cr^{3+}, Fe^{3+}, Cu^{2+}, and Zn^{2+} enhances the porphyrin emission, particularly for Cr^{3+} (1.5-fold), Fe^{3+} (3.7-fold) and Zn^{2+} (2.4-fold). Turning to the NIR emission intensity, Na^+ and Zn^{2+} have almost no effect, while the other ions decrease it, marginally for Mg^{2+}, Ca^{2+}, Co^{2+}, and Cu^{2+} (∼12%-25%), ∼30% for Cr^{3+}, and > 99% for Fe^{3+}. The large quenching effect from Fe^{3+} probably arises from a strong interaction of this ion with the porphyrin, leading to Yb^{3+} dissociation.

Regarding the Schiff base complex **NdL3**, the addition of Na^+, K^+, and Mg^{2+} has no influence on the ligand emission intensity, while only Mg^{2+} quenches the metal ion luminescence (∼13%), indicating the preservation of the complex structure. However, the addition of Ca^{2+} decreases the NIR emission by ∼69% while largely enhancing (tenfold) the ligand emission at 450 nm,

TABLE 1 | Experimental stability constants for LnL1 and LnL2 complexes and corresponding data for LnL2 [22, 27] and LnL4 [28].

Stability constants log K_C				
Ln	**L1 [a] (this work)**	**L2 [b] (Ref. 22)**	**L3 [c] (this work)**	**L4 [d] (Ref. 31)**
Nd	n.d.	23.0	4.82 ± 0.20	15.75 ± 0.06
Gd	17.30 ± 0.02	24.7	4.97 ± 0.07	16.28 ± 0.06
Er	18.91 ± 0.03	24.4	n.d.	17.45 ± 0.06
Yb	21.11 ± 0.11	25.0	5.12 ± 0.13	18.04 ± 0.07

[a]Standard deviation calculated on triplicate repeat experiments. Equilibrium at 37°C in PBS buffer (0.1 M NaCl, pH 7.5).
[b] Spectrophotometric measurement in 0.01 M acetate buffer, 0.1 M NaCl, pH 3.89; room temperature.
[c] Standard deviation calculated on triplicate repeat experiments. Measurement at room temperature, in water at pH 7.
[d] Potentiometric titration in 0.50 M $NaClO_4$ at 25°C.

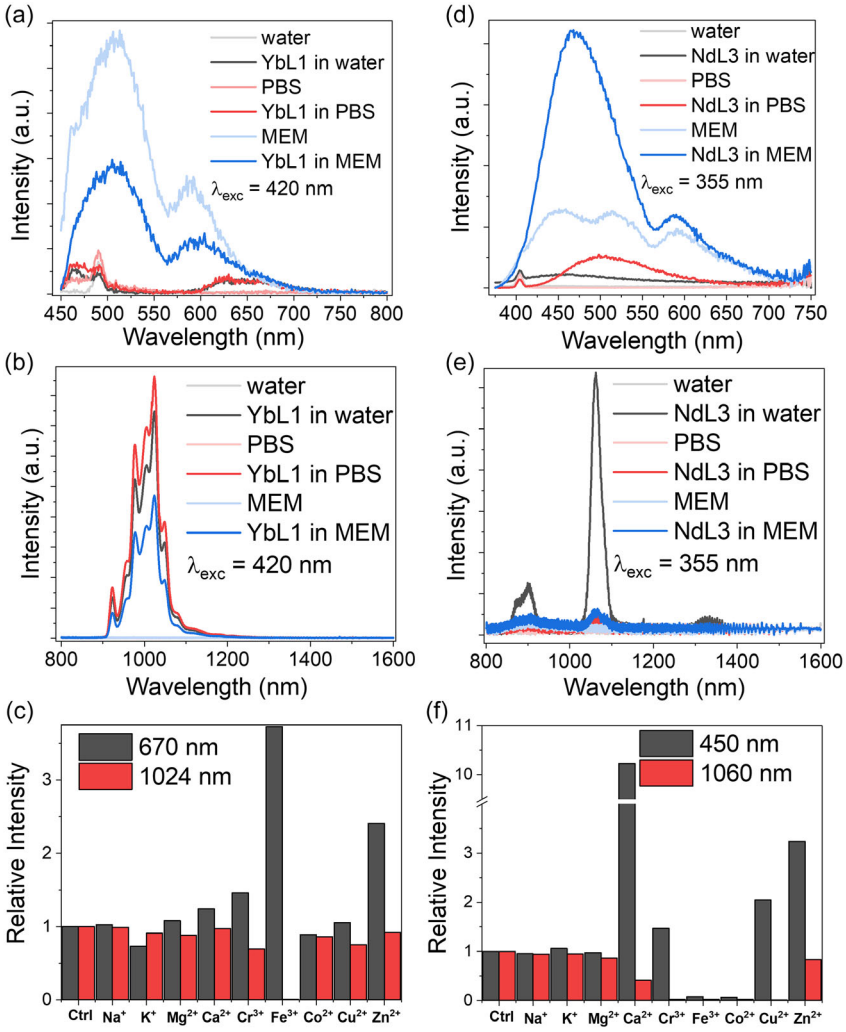

FIGURE 3 | Emission spectra of (a), (b), (c) **YbL1** (10 μM, 0.1%DMSO), and (d), (e), (f) **NdL3** (50 μM, 0.5%DMSO), in different solvents and in presence of different potentially interfering ions (5 mM); (a), (b) ligand emission; (b), (e) Ln^{3+} emission; (c), (f) black bars: ligand emission, red bars: Ln^{3+} emission.

pointing to Ca^{2+} replacing Nd^{3+}. The addition of Zn^{2+} has similar but much less important effects with the 450-nm emission enhanced ~threefold and the NIR emission decreased by ~ 17%; we interpret these data as arising from partial displacement of Nd^{3+}. The transition metal ions all substantially quench the Nd^{3+} emission while inducing diverse effects on the ligand emission, with Cr^{3+} and Cu^{2+} increasing it, and Fe^{3+} and Co^{2+} quenching it. This translates to the Nd^{3+} complex being dissociated upon competition with these ions.

To further test the stability of the lanthanide porphyrin complexes, we have titrated them with trivalent iron. Unlike the Yb^{3+} complex, the Gd^{3+} and Er^{3+} porphyrin complexes did not display the metal-centered luminescence due to the unmatched energy level. Therefore, the effect of Fe^{3+} was unraveled by monitoring the intensity of the excitation spectrum of the 670-nm ligand emission band. The excitation band at around 450 nm increases with increasing Fe^{3+}concentration, while the intensity of the 400-nm band decreases, which indicates the formation of an iron–porphyrin complex. This was confirmed by titrating the porphyrin ligand (**L1**) with Fe^{3+} (Figure 4). The trend of change follows the trend of stability constants. The more stable the lanthanide complex is, the smaller the difference between the excitation pattern changes. However, the change only happens at high iron concentrations with a molecular ratio greater than 100, which is in line with the large stability constant of **LnL1**.

To further test the imaging potential of the studied lanthanide complexes, luminescence titrations with human serum albumin (HSA) were performed (Figure 5).

Regarding the stable complex **YbL1**, the addition of HSA up to 10 equivalents did not reduce the NIR emission, meaning that the complex structure was maintained. The increasing emission at around 470 nm (Figure S34) is due to the increasing concentration of free HSA during the titration process. Conversely, the porphyrin emission at 670 nm remains constant, pointing to the non-dissociation of the macrocyclic complex. These results indicate that the imaging ability of **YbL1** will not be affected by serum proteins such as HSA.

On the contrary, the addition of HSA to **NdL3** resulted in a large variation of the emission intensity (Figure 5d-f). As soon as HSA is added to the solution, Nd^{3+} luminescence increases sharply up to a [HSA]/[NdL3] ratio of 0.1, for which the intensity is fivefold the initial one. But with further HSA addition, the Nd^{3+} emission constantly decreases to reach 24% of the

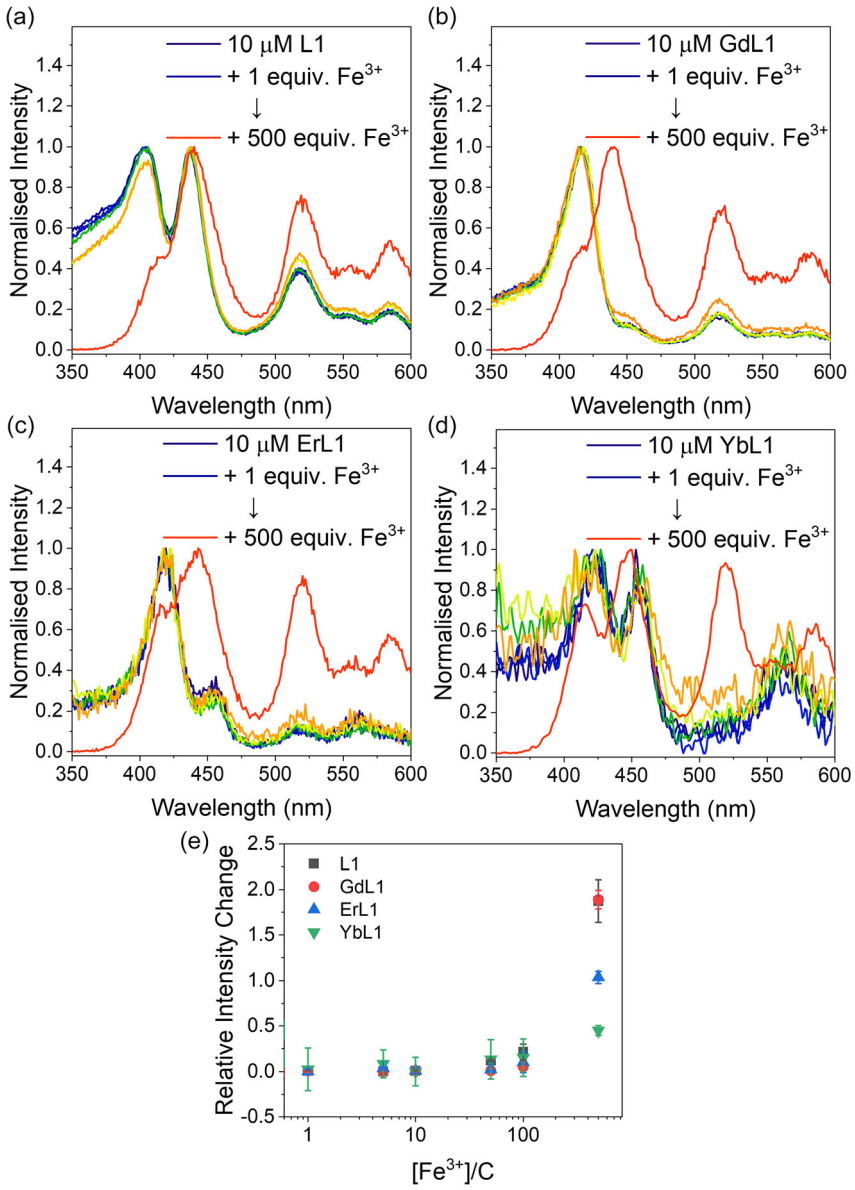

FIGURE 4 | Luminescence titration of **L1** and **LnL1** complexes by Fe^{3+} : **L1** (a), **GdL1** (b), **ErL1** (c), and **YbL1** (d) (10 μM in 20 mM Tris, 150 mM NaCl, pH 7.5, $\lambda_{em} = 670$ nm). (e) Relative intensity change upon addition of Fe^{3+}, C = [**L1**] or [**LnL1**], Relative Intensity Change = $I_{450nm}/I_{420nm} - I_{450nm}/I_{420nm}$ at $[Fe^{3+}] = 0$.

initial intensity. Figure S35–36 shows the emission spectra 5, 10, and 15 min after HSA addition, pointing to the fast reaching of the chemical equilibrium. In parallel, the ligand emission intensity steadily increases up to a [HSA]/[**NdL3**] ratio of 1.5 and then stabilizes. Initial interaction of HSA favors energy transfer onto the Nd^{3+} ion, but the **NdL3**-HSA resultant conjugate rearranges, and transmetallation occurs, indeed, HSA is the main carrier of Zn^{2+} in blood plasma and has, therefore, a high affinity for this ion.

The above results clearly emphasize the importance of assessing bioprobe stability when used for luminescence imaging since both biomolecules, such as proteins, or common metal ions present in the plasma and other biological fluids, such as iron, will otherwise interfere and, at least partially, destroy the probe. During measurement of the stability constants, complexation kinetics must be considered; that is, the stability constants should be determined at equilibrium. In addition, experimental conditions like temperature [13], ionic strength [32], and pH [33] also influence the stability of the metal complexes.

3 | Experimental

3.1 | Photophysical Properties

UV–visible absorption spectra in the spectral range 200–1100 nm were recorded with an HP Agilent UV-8453 spectrophotometer. A Horiba Fluorolog-3 spectrophotometer setup equipped with a visible to near-infrared-sensitive photomultiplier in a nitrogen flow-cooled housing was used for both luminescence lifetime and steady-state emission measurements. All data were processed with Origin 2021 from OriginLab.

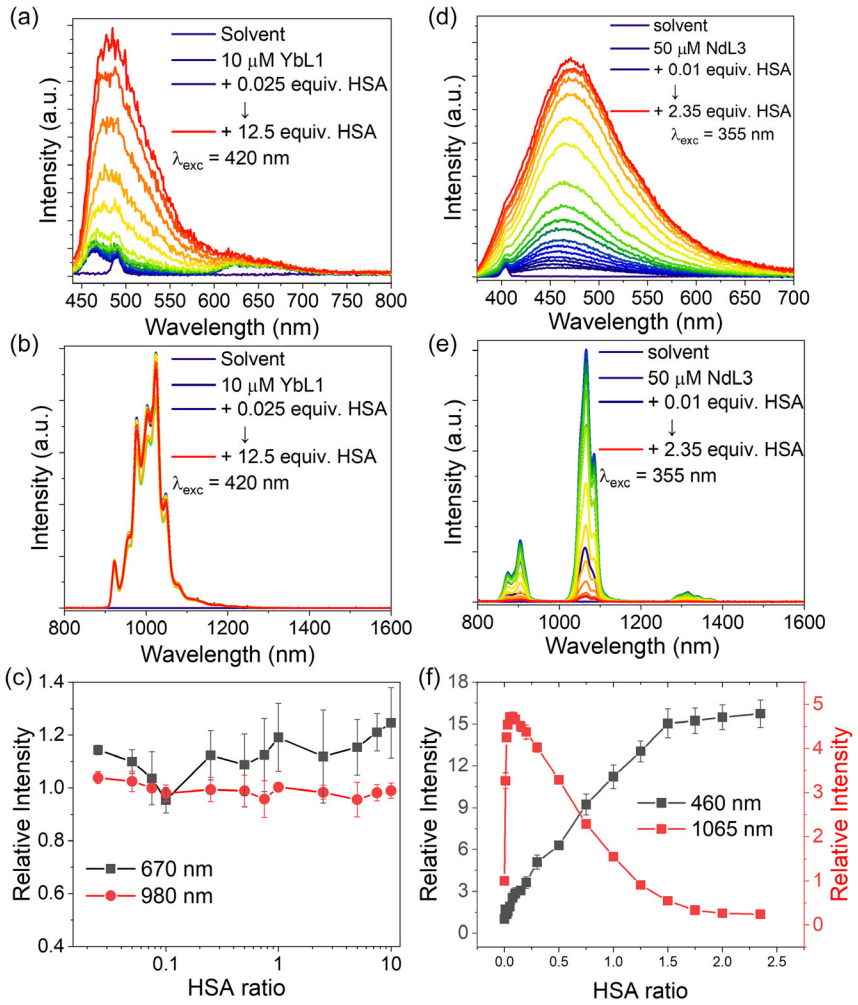

FIGURE 5 | Luminescent titration of **LnL1** complexes with HSA (20 mM Tris buffer, 150 mM NaCl, pH 7.5). Emission spectrum of **YbL1** (10 μM) in the visible (a) and NIR (b) with the addition of HSA, and summarized trend (c). Emission spectrum of **NdL3** (50 μM) in the visible (d) and NIR (e) with the addition of HSA, and summarized trend (f).

3.2 | Stability Constants

3.2.1 | LnL1: Competitive Titrations With EDTA

Reactions were performed in phosphate buffer solutions (PBS, pH 7.4) and were monitored by UV–visible spectroscopy until equilibrium was reached. Typically, 3 ml solutions of LnL1 10 μM in PBS containing different amounts of Na4-EDTA (0–1 mM for GdL1, 0–10 mM for ErL1, and 0–15 mM for YbL1) were shaken for longer than 90 days to reach equilibrium. Absorption bands at 422 (L1) and 441 nm (LnL1) were monitored. There is some overlap between these bands, so a correction had to be applied considering the molar absorption coefficients of each species. To increase accuracy, another pair of absorption bands at 519 and 564 nm was included in the calculations performed with OriginLab 2021. All experiments were conducted in triplicate.

Stability constants were calculated as follows. The formation equilibrium of a 1:1 complex, described by the chemical equation

$$M + L \rightleftharpoons [ML] \tag{1}$$

is characterized by the corresponding association (Equation (2)) or dissociation (Equation (3)) constants

$$K_a = \frac{[ML]}{[M] \times [L]} \tag{2}$$

$$K_d = \frac{[M] \times [L]}{[ML]} = \frac{1}{K_a} \tag{3}$$

In case of competition with a second ligand L', Equation (1) becomes

$$[ML] + L' \rightleftharpoons [ML'] + L \tag{4}$$

can be derived from Equation (3) :

$$\frac{K_d}{K_d'} = \frac{[M] \times [L]}{[ML]} \div \frac{[M] \times [L']}{[ML']} \tag{5}$$

After mathematical rearrangement, the relationship between the stability constants of the two complexes can be written as:

$$log\frac{[ML']}{[ML]} + logK_D = log\frac{[L']}{[L]} + logK_D' \tag{6}$$

Since the concentration of the newly formed metal complex with the competing ligand is equal to the concentration reduction of

the original complex, the logarithm of their quotient is 0. The relationship between the known stability constant and the stability constant of interest is, therefore:

$$logK_D = log\frac{[L']}{[L]} + logK'_{D'} \quad (7)$$

After calculation of the actual concentration of complex and ligand with different additions of EDTA, the logarithm of the ratio between the concentrations of Gd-EDTA (with known pK_D) and GdL1 (with unknown pK_D) was plotted against the logarithm of the quotient between the concentrations of EDTA and L1 according to Equation (6) [34]. When the concentrations of the 2 metal complexes are equal, the log of their quotient is 0, and the stability constant can be easily calculated.

3.2.2 | LnL3: Direct Method

Solutions of propylene(C3)-Zn-Nd-salen (50 μM in Milli Q water) were prepared in 1-month time interval. The absorption and emission spectra in the visible and NIR were obtained with the HP Agilent UV-8453 spectrophotometer. The absorption spectra were monitored at 345 nm; experiments were made in triplicate.

3.3 | Interference Determination

All experiments were conducted in triplicate. 3 mL of solutions of LnL3 (10 μM for Yb, 50 μM for Nd) containing 5 mM of different metal chlorides (NaCl, KCl, $MgCl_2$, $CaCl_2$, $ZnCl_2$, $CuCl_2$, $CoCl_2$, $CrCl_3$, $FeCl_3$) were shaken for 3 days. Emission spectra were recorded in both visible and NIR spectral ranges.

3.4 | Luminescent Titration With HSA

To a 2.5 mL solution of lanthanide complex (10 μM for YbL1, 50 μM for NdL3) in TBS, HSA was added gradually. The emission spectra were recorded in both visible and NIR spectral ranges.

3.5 | Luminescent Titration With Fe^{3+}

3 mL of solutions of LnL1 and L1 (10 μM) were reacted with various concentrations of $FeCl_3$ (0, 10, 50, 100, 500, 1000, and 5000 μM), respectively. Emission spectra were recorded in both visible and NIR spectral ranges.

4 | Conclusion

The stability constants for lanthanide monoporphyrinates capped with Kläui's ligand were determined for the first time. The **LnL1** complexes exhibit slightly higher thermodynamic stability than Ln-EDTA complexes (by 1–3 orders of magnitude), which might be due to the pre-organized coordinating ring and to the capping ligand. On the other hand, despite their favorable encapsulation of the lanthanide ions, these complexes remain 4–7 orders of magnitude less stable than the corresponding Ln-DOTA complexes. A second point dealt with in this work is the luminescence behavior of the **LnL1** and **LnL3** complexes toward the addition of common metal ions within the framework of potential imaging experiments. The response depends heavily on the nature of the interfering ion and protein, and therefore careful consideration of the medium in which the bioimaging experiments are to be performed should be made.

Acknowledgments

KLW acknowledges financial support from RGC Areas of Excellence (AoE/M-401/20), NSFC/RGC Joint Research Scheme (N_PolyU209/21), and Innovation and Technology Fund - Partnership Research Programme (PRP/040/23FX). The authors also appreciate the service of the mass spectrometry facility provided by the University Research Facility in Life Sciences (ULS) of HKPolyU.

Funding

This work was supported by Research Grants Council, University Grants Committee(AoE/M-401/20), NSFC/RGC Joint Research Scheme(N_PolyU209/21), Innovation and Technology Fund(PRP/040/23FX).

Conflicts of Interest

The authors have no conflict of interest.

Data Availability Statement

The data that supports the findings of this study are available in the supplementary material of this article.

References

1. P. Lei, J. Feng, and H. Zhang, "Emerging Biomaterials: Taking Full Advantage of the Intrinsic Properties of Rare Earth Elements," *Nano Today* 35 (2020): 100952.

2. J.-C. G. Bünzli, "On the Design of Highly Luminescent Lanthanide Complexes," *Coordination Chemistry Reviews* 293-294 (2015): 19–47.

3. M. C. Heffern, L. M. Matosziuk, and T. J. Meade, "Lanthanide Probes for Bioresponsive Imaging," *Chemical Reviews* 114 (2014): 4496–4539.

4. S. Wheeler and S. J. Butler, "Exploiting the Unique Properties of Lanthanide Complexes as FRET Probes: From Quantitation to Protein Dynamics," *Analysis & Sensing* 3 (2023): e202200036.

5. J. Wahsner, E. M. Gale, A. Rodríguez-Rodríguez, and P. Caravan, "Chemistry of MRI Contrast Agents: Current Challenges and New Frontiers," *Chemical Reviews* 119 (2019): 957–1057.

6. S. P. Fricker, "The Therapeutic Application of Lanthanides," *Chemical Society Reviews* 35 (2006): 524–533.

7. J. Fallah, S. Agrawal, H. Gittleman, et al., "FDA Approval Summary: Lutetium Lu 177 Vipivotide Tetraxetan for Patients with Metastatic Castration-Resistant Prostate Cancer," *Clinical Cancer Research : an Official Journal of the American Association for Cancer Research* 29 (2023): 1651–1657.

8. G. Pagano, P. J. Thomas, A. Di Nunzio, and M. Trifuoggi, "Human Exposures to Rare Earth Elements: Present Knowledge and Research Prospects," *Environmental Research* 171 (2019): 493–500.

9. S. E. Cowper and R. Bucala, "Nephrogenic Fibrosing Dermopathy: Suspect Identified, Motive Unclear," *The American Journal of Dermatopathology* 25 (2003): 357–362.

10. M. Constantin, M. F. Chioncel, L. Petrescu, et al., "From Rock to Living Systems: Lanthanides Toxicity and Biological Interactions," *Ecotoxicology and Environmental Safety* 289 (2025): 117494.

11. H. Herrmann, J. Nolde, S. Berger, and S. Heise, "Aquatic Ecotoxicity of Lanthanum - A Review and an Attempt to Derive Water and Sediment

Quality Criteria," *Ecotoxicology and Environmental Safety* 124 (2016): 213–238.

12. J. Barańska, K. Koroniak-Szejn, M. Zabiszak, et al., "Potentiometric Studies of the Complexation Properties of Selected Lanthanide Ions with Schiff Base Ligand," *International Journal of Molecular Sciences* 26 (2025): 10379.

13. V. D. Athawale and V. Lele, "Stability Constants and Thermodynamic Parameters of Complexes of Lanthanide Ions and (±)-Norvaline," *Journal of Chemical and Engineering Data* 41 (1996): 1015–1019.

14. M. T. Kaczmarek, M. Zabiszak, M. Nowak, and R. Jastrzab, "Lanthanides: Schiff Base Complexes, Applications in Cancer Diagnosis, Therapy, and Antibacterial Activity," *Coordination Chemistry Reviews* 370 (2018): 42–54.

15. G.-Q. Jin, C. V. Chau, J. F. Arambula, S. Gao, J. L. Sessler, and J.-L. Zhang, "Lanthanide Porphyrinoids as Molecular Theranostics," *Chemical Society Reviews* 51 (2022): 6177–6209.

16. W.-L. Chan, C. Xie, W.-S. Lo, J.-C. G. Bünzli, W.-K. Wong, and K.-L. Wong, "Lanthanide-Tetrapyrrole Complexes: Synthesis, Redox Chemistry, Photophysical Properties, and Photonic Applications," *Chemical Society Reviews* 50 (2021): 12189–12257.

17. J.-C. G. Bünzli, "Review: Lanthanide Coordination Chemistry: From Old Concepts to Coordination Polymers," *Journal of Coordination Chemistry* 67 (2014): 3706–3733.

18. W. Kläui, "The Coordination Chemistry and Organometallic Chemistry of Tridentate Oxygen Ligands with π-Donor Properties," *Angewandte Chemie International Edition* 29 (1990): 627–637.

19. T. D. Pasatoiu, A. M. Madalan, M. Zamfirescu, C. Tiseanu, and M. Andruh, "One- and Two-Photon Induced Emission in Heterobimetallic Zn(II)-Sm(III) and Zn(II)-Tb(III) Complexes with a Side-Off Compartmental Ligand," *Physical Chemistry Chemical Physics* 14 (2012): 11448–11456.

20. N. Dwivedi, S. K. Panja, A. Verma, et al., "NIR Luminescent Heterodinuclear [ZnII LnIII] Complexes: Synthesis, Crystal Structures and Photophysical Properties," *Journal of Luminescence* 192 (2017): 156–165.

21. W.-K. Lo, W.-K. Wong, W.-Y. Wong, et al., "Heterobimetallic Zn(II)–Ln(III) Phenylene-Bridged Schiff Base Complexes, Computational Studies, and Evidence for Singlet Energy Transfer as the Main Pathway in the Sensitization of Near-Infrared Nd3+ Luminescence," *Inorganic Chemistry* 45 (2006): 9315–9325.

22. W. P. Cacheris, S. K. Nickle, and A. D. Sherry, "Thermodynamic Study of Lanthanide Complexes of l,4,7-Triazacyclononane-N, N', N"-Triacetic Acid and 1.4.7.10- Tetraazacyclododecane-N, N', N," *Inorganic Chemistry* 26 (1987): 958–960.

23. R. M. Smith and A. E. Martell, *Critical Stability Constants*. New York, NY: Springer, 1976, 4.

24. C. Li, Y. Pang, Y. Xu, et al., "Near-Infrared Metal Agents Assisting Precision Medicine: From Strategic Design to Bioimaging and Therapeutic Applications," *Chemical Society Reviews* 52 (2023): 4392–4442.

25. E. D. Suarez, F. C. D. A. Lima, P. M. Dias, V. R. L. Constantino, and H. M. Petrilli, "Theoretical UV-Vis Spectra of Tetracationic Porphyrin: Effects of Environment on Electronic Spectral Properties," *Journal of Molecular Modeling* 25 (2019): 264.

26. Y. Luo, Z. Liu, H. T. Wong, et al., "Energy Transfer between Tb(3+) and Eu(3+) in LaPO(4): Pulsed versus Switched-Off Continuous Wave Excitation," *Advancement of Science* 6 (2019): 1900487.

27. Ė. Tóth and E. Brücher, "Stability Constants of the Lanthanide(III)-1,4,7,10-Tetraazacyclododecane-N, N′, N″, N‴-Tetraacetate Complexes," *Inorganica Chimica Acta* 221 (1994): 165–167.

28. T. F. Gritmon, M. P. Goedken, and G. R. Choppin, "The Complexation of Lanthanides by Aminocarboxylate Ligands—I: Stability Constants," *Journal of Inorganic and Nuclear Chemistry* 39 (1977): 2021–2023.

29. F.-F. Chen, Z.-Q. Chen, Z.-Q. Bian, and C.-H. Huang, "Sensitized Luminescence From Lanthanides in d–f Bimetallic Complexes," *Coordination Chemistry Reviews* 254 (2010): 991–1010.

30. J. M. Van Raden, D. I. Alexandropoulos, M. Slota, et al., "Singly and Triply Linked Magnetic Porphyrin Lanthanide Arrays," *Journal of the American Chemical Society* 144 (2022): 8693–8706.

31. P. D'Angelo, A. Zitolo, V. Migliorati, et al., "Revised Ionic Radii of Lanthanoid(III) Ions in Aqueous Solution," *Inorganic Chemistry* 50 (2011): 4572–4579.

32. F. J. Millero, "Stability Constants for the Formation of Rare Earth-Inorganic Complexes as a Function of Ionic Strength," *Geochimica et Cosmochimica Acta* 56 (1992): 3123–3132.

33. P. Mandal, J. Kretzschmar, and B. Drobot, "Not Just a Background: PH Buffers Do Interact with Lanthanide Ions-a Europium(III) Case Study," *JBIC Journal of Biological Inorganic Chemistry* 27 (2022): 249–260.

34. D. M. J. Doble, M. Melchior, B. O'Sullivan, et al., "Toward Optimized High-Relaxivity MRI Agents: The Effect of Ligand Basicity on the Thermodynamic Stability of Hexadentate Hydroxypyridonate/Catecholate Gadolinium(III) Complexes," *Inorganic Chemistry* 42 (2003): 4930–4937.

Supporting Information

Additional supporting information can be found online in the Supporting Information section.